

# Accepted Manuscript

Inhibiting A $\beta$  toxicity in Alzheimer's disease by a pyridine amine derivative

Zhenzhu Zhu, Tao Yang, Lei Zhang, Lulu Liu, Enmao Yin, Changli Zhang, Zijian Guo, Chen Xu, Xiaoyong Wang



PII: S0223-5234(19)30166-7

DOI: <https://doi.org/10.1016/j.ejmech.2019.02.052>

Reference: EJMECH 11144

To appear in: *European Journal of Medicinal Chemistry*

Received Date: 12 December 2018

Revised Date: 7 February 2019

Accepted Date: 17 February 2019

Please cite this article as: Z. Zhu, T. Yang, L. Zhang, L. Liu, E. Yin, C. Zhang, Z. Guo, C. Xu, X. Wang, Inhibiting A $\beta$  toxicity in Alzheimer's disease by a pyridine amine derivative, *European Journal of Medicinal Chemistry* (2019), doi: <https://doi.org/10.1016/j.ejmech.2019.02.052>.

This is a PDF file of an unedited manuscript that has been accepted for publication. As a service to our customers we are providing this early version of the manuscript. The manuscript will undergo copyediting, typesetting, and review of the resulting proof before it is published in its final form. Please note that during the production process errors may be discovered which could affect the content, and all legal disclaimers that apply to the journal pertain.

# Graphical abstract

## Inhibiting A $\beta$ Toxicity in Alzheimer's Disease by a Pyridine Amine

### Derivative

Zhenzhu Zhu<sup>a, 1</sup>, Tao Yang<sup>a, 1</sup>, Lei Zhang<sup>a</sup>, Lulu Liu<sup>a</sup>, Enmao Yin<sup>a</sup>, Changli Zhang<sup>b</sup>,  
Zijian Guo<sup>c</sup>, Chen Xu<sup>a, \*</sup>, and Xiaoyong Wang<sup>a, \*</sup>

<sup>a</sup>State Key Laboratory of Pharmaceutical Biotechnology, School of Life Sciences, Nanjing University, Nanjing 210023, P. R. China

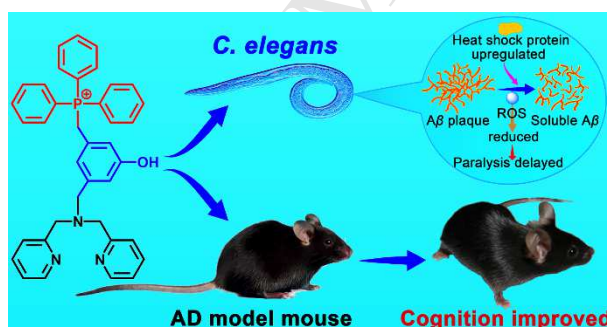
<sup>b</sup>State Key Laboratory of Coordination Chemistry, School of Chemistry and Chemical Engineering, Nanjing University, Nanjing 210023, P. R. China

<sup>c</sup>Department of Chemistry, Nanjing Xiaozhuang College, Nanjing 210017, P. R. China

\* Corresponding author. State Key Laboratory of Pharmaceutical Biotechnology, School of Life Sciences, Nanjing University, Nanjing 210023, P. R. China.

*E-mail addresses:* boxwxy@nju.edu.cn (X. Y. Wang), xuchn@nju.edu.cn (C. Xu)

<sup>1</sup>These authors contributed equally to this work.



# Inhibiting $A\beta$ toxicity in Alzheimer's disease by a pyridine amine derivative

Zhenzhu Zhu<sup>a,#</sup>, Tao Yang<sup>a,#</sup>, Lei Zhang<sup>a</sup>, Lulu Liu<sup>a</sup>, Enmao Yin<sup>a</sup>, Changli Zhang<sup>b</sup>, Zijian Guo<sup>c</sup>, Chen Xu<sup>a,\*</sup>, and Xiaoyong Wang<sup>a,\*</sup>

<sup>a</sup> State Key Laboratory of Pharmaceutical Biotechnology, School of Life Sciences, Nanjing University, Nanjing 210023, P. R. China

<sup>b</sup> Department of Chemistry, Nanjing Xiaozhuang College, Nanjing 210017, P. R. China

<sup>c</sup> State Key Laboratory of Coordination Chemistry, School of Chemistry and Chemical Engineering, Nanjing University, Nanjing 210023, P. R. China

\* Corresponding author. E-mail addresses: boxwxy@nju.edu.cn (X. Y. Wang), xuchn@nju.edu.cn (C. Xu)

# These authors contributed equally to this work.

## Abstract

Alzheimer's disease (AD) is a neurodegenerative disorder with no radical therapy. Aggregation of amyloid  $\beta$ -peptide ( $A\beta$ ) induced by various factors is associated with pathogenesis of AD. A pyridine amine derivative, 3-bis(pyridin-2-ylmethyl)aminomethyl-5-hydroxybenzyltriphenylphosphonium bromide (PAT), is synthesized. The inhibition of self- and metal-induced  $A\beta$  aggregation by PAT is confirmed by thioflavine T fluorescence, circular dichroism spectroscopy, and TEM. Western blot, RT-PCR and fluorescence imaging indicate that PAT can alleviate the  $A\beta$ -induced paralysis, reduce the production of ROS, and protect the mitochondrial function in transgenic *C. elegans*. Genetic analyses indicate that heat shock protein is involved in the alleviation of  $A\beta$  toxicity. PAT also inhibits the activity of acetylcholinesterase in *C. elegans*. Morris water maze test shows that the memory and cognitive ability of APP/PS1 AD model mice are significantly

improved by PAT. Both *in vitro* and *in vivo* studies demonstrate that PAT is effective in counteracting  $A\beta$  toxicity and ameliorating cognitive functions in AD mice, and therefore a potential lead compound of anti-AD drugs.

**Keywords:** Alzheimer's disease • amyloid- $\beta$  peptide • anti-AD drug • heat shock protein • *Caenorhabditis elegans*

## 1. Introduction

Alzheimer's disease (AD) is a devastating neurodegenerative disorder encountered frequently by elderly people in the world [1, 2]. Although some small molecules, such as inhibitors of  $\gamma$ -secretase,  $\beta$ -secretase, tau aggregation or microglial activation, and immunotherapeutic agents targeting at amyloid- $\beta$  peptide ( $A\beta$ ) and p-tau clearance are in clinical trials [3], only five drugs are approved by the FDA for the treatment of AD [4]. Even so, no disease-modifying treatment that can halt or slow the progression of AD is available up to now [5, 6].

The exact molecular mechanism leading to AD remains unclear; however, a growing body of evidence implicates that AD is caused by multiple factors, such as  $A\beta$  aggregation, tau-protein hyperphosphorylation, oxidative stress and acetylcholine breakdown [7]. Among them, the  $A\beta$  aggregation plays a major role in neural loss and cognitive impairment by forming senile plaques; it also relates to the increased oxidative stress responsible for the neuronal injury and death [8]. The high level of  $A\beta$  in the AD brain came from the abnormal cleavage of amyloid precursor protein (APP) by  $\beta$ - and  $\gamma$ -secretases, which gives  $A\beta_{40}$  and  $A\beta_{42}$  containing 40 and 42 amino acid residues respectively [9]. These  $A\beta$  species form unbranched fibrils consisting of parallel and orderly  $\beta$ -sheet structures [10].  $A\beta$ , especially  $A\beta_{42}$ , is prone to form toxic aggregates [11]; among them, soluble  $A\beta$  oligomers are the main cytotoxic species [12]. Therefore, preventing  $A\beta$  aggregation is a major strategy against AD; beyond this, reducing oxidative stress, or activating disease-modifying pathways could also relieve the onset of AD [13].

On the other side, AD is recognized to be linked to the function and status of metal ions, such as  $\text{Cu}^{2+}$ ,  $\text{Zn}^{2+}$  or  $\text{Fe}^{2+}$  [14]. These ions are present at high concentrations in  $A\beta$  plaques ( $\text{Cu}^{2+}$   $\sim$ 400  $\mu\text{M}$ ,  $\text{Zn}^{2+}$   $\sim$ 1 mM,  $\text{Fe}^{2+}$   $\sim$ 1 mM), which contribute to the stability of  $A\beta$  aggregates [15], the production of reactive oxygen species (ROS), and the loss of neuronal function [16]. Thus, rebalancing the metal ions and relieving oxidative stress in AD pathogenesis is becoming a potential strategy for the therapy of AD [17, 18].

Transgenic caenorhabditis elegans (*C. elegans*) that expresses human  $A\beta$  gene has been used as a model system to mimic AD in order to probe the molecular mechanism of  $A\beta$  toxicity [19] and screen therapeutic agents [20], because it has a short lifespan, well-characterized genome and considerable homology with human genomes [21]. Transgenic worms, such as CL4176 and GMC101, were genetically engineered to express the human  $A\beta_{42}$  gene in muscle cells [22]. The accumulation of  $A\beta$  species in *C. elegans* muscle cells results in either a progressive or a rapid paralytic phenotype, providing a simple biological readout of  $A\beta$  toxicity [23]. It was reported that overexpression of heat shock protein or factors could suppress  $A\beta$  toxicity by interacting directly with  $A\beta$  and altering its oligomerization pathways, thereby reducing the formation of toxic species in *C. elegans* [24, 25].

Multifunctional compounds containing metal chelating moieties, such as 8-hydroxyquinoline, polyphenols, flavonoids and pyridine amine derivatives, have been reported as potential anti-AD agents [26]. For example, pyridine amine derivative in Fig. 1 forms stable metal complexes by incorporating N,N,O donor atoms; moreover, it shows anti-oxidative activity due to the presence of phenolic group [27]. These compounds interact with  $\text{Cu}^{2+}$  and  $\text{Zn}^{2+}$  to disaggregate the metal-associated  $A\beta$  aggregates. On the other hand, lipophilic cations such as triphenylphosphonium ( $\text{TPP}^+$ ) derivatives are rapidly and extensively taken up by mitochondria due to large mitochondrial membrane potential (MMP) [28]. Covalent attachment of  $\text{TPP}^+$  has been proven to be a robust method to target small and

bioactive molecules to mitochondria [29]. For example, mitoquinone (MitoQ) is a mitochondrion-targeted antioxidant designed to protect against oxidative damage within mitochondria and has undergone clinical trials in humans [30].

Considering the advantages of multifunctional compounds, a pyridine amine derivative, 3-bis(pyridin-2-ylmethyl)aminomethyl-5-hydroxybenzyltriphenylphosphonium bromide (PAT), was designed in this study (Fig. 1). The presence of phenolic group and mitochondrion-targeted TPP moiety in PAT may protect against the oxidative damage in mitochondria. Cell-free studies showed that PAT could inhibit the self-assembly of  $A\beta$  fibrils and  $Zn^{2+}/Cu^{2+}$ -induced  $A\beta$  aggregation; in  $A\beta$ -transgenic *C. elegans*, it dramatically delayed the progression of body paralysis, reduced the amount of  $A\beta$  species and oxidative activity. More importantly, PAT played a prominent role in protecting against  $A\beta$  toxicity and maintaining healthy proteostasis in AD worms. As a result, the cognitive and memory abilities of APP/PS1 AD mice were significantly improved after PAT treatment.

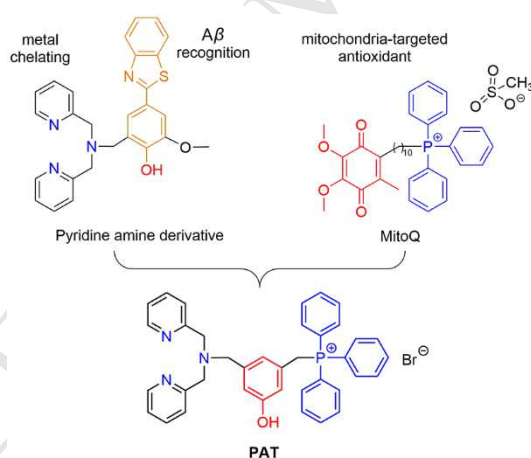


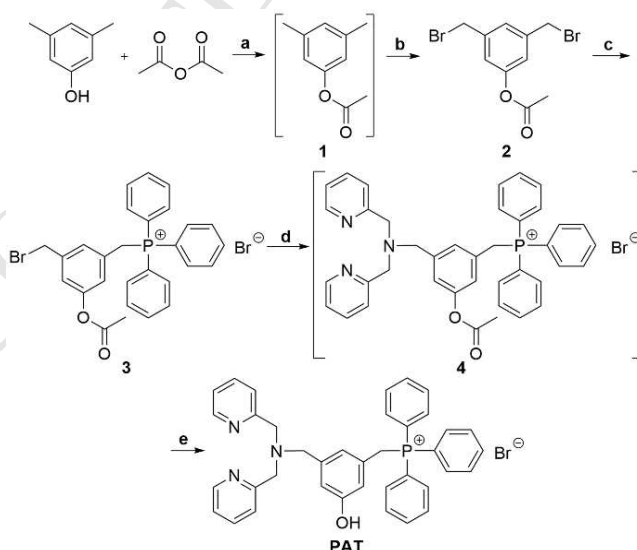
**Fig. 1.** Structures of PAT and its parents.

## 2. Results and discussion

### 2.1. Design and characterization

The synthetic route to PAT was shown in Scheme 1. The compound was characterized by  $^1H$ ,  $^{31}P$  NMR and ESI-MS spectroscopy (Fig. S1).

Bis(2-pyridylmethyl)amine was selected as the chelating moiety because its binding ability to  $\text{Cu}^{2+}$  and  $\text{Zn}^{2+}$  ( $\log K_{\text{Cu}} = 9.3$ ;  $\log K_{\text{Zn}} = 7.6$ ) [31] is moderately higher than that for  $\text{A}\beta_{40}$  ( $\log K_{\text{Cu}} = 5-9$ ;  $\log K_{\text{Zn}} = 3-7$ ) [32, 33]. Lipophilicity is an important parameter influencing a compound to penetrate the cellular membrane and blood-brain barrier (BBB). Thus, lipophilic triphenylphosphonium cation ( $\text{TPP}^+$ ) was used to improve the lipophilicity of PAT and facilitate its accumulation in mitochondria owing to the characteristic of MMP (180–200 mV, negative inside) [34]. In view of the potential anti-oxidative activity, 3,5-bis(bromomethyl)phenol was selected to link the two functional moieties. We suppose that PAT may have several properties favorable for AD treatment: (i) inhibiting metal-induced  $\text{A}\beta$  aggregation through the chelating moiety; (ii) enhancing the BBB-penetrating power via the TPP lipophilic cation; and (iii) reducing the oxidative stress by the phenolic group. Although the molecular weight (580.69, without  $\text{Br}^-$ ) and  $\text{Clog}P$  (7.51) are larger than those suggested by the Lipinski' rules (Table S1) [35], we still expect that PAT could cross the BBB due to its poor water solubility. To ensure the BBB penetration of PAT, dimethylsulfoxide (DMSO) was used in the *in vivo* studies to realize the solvent-mediated disruption to the membrane [36].



**Scheme 1.** Synthetic route to PAT. Reagents and conditions: (a) pyridine, rt, 48 h; (b) NBS, BPO,  $\text{CCl}_4$ ; (c) triphenylphosphine,  $\text{CCl}_4$ , rt, overnight; (d)

bis(2-pyridylmethyl)amine, DIEA,  $\text{CHCl}_3$ , rt, 48 h; (e) NaOH, HCl,  $\text{CH}_3\text{OH}/\text{H}_2\text{O}$ .

## 2.2. Inhibition of $A\beta$ aggregation

Metal ions such as  $\text{Zn}^{2+}$  and  $\text{Cu}^{2+}$  can interact with  $A\beta$  and facilitate its aggregation, producing toxic oligomeric peptide species [14]. The effect of PAT on the  $A\beta$  aggregation was investigated using thioflavine T (ThT) because it can specifically bind to the aggregated  $\beta$ -sheet fibrils common to amyloid structures and emit enhanced fluorescence [37]. As presented in Fig. 2A, the fluorescence intensity of ThT decreases dramatically when PAT is added to the solution of  $\text{Zn}^{2+}$ - or  $\text{Cu}^{2+}$ - $A\beta_{40}$  aggregates. The most potent effect of PAT on the  $\text{Zn}^{2+}$ -induced  $A\beta_{42}$  aggregation was observed at the half maximal inhibitory concentration ( $\text{IC}_{50}$ ) of  $27.42 \pm 1.52 \mu\text{M}$  (Fig. 2B). In the progression of AD, part of  $A\beta$  switches from a nontoxic  $\alpha$ -helix to a toxic  $\beta$ -sheet conformation, forming self-assembled aggregates and leading to neurotoxicity [38]. ThT assay indicates that the  $\text{IC}_{50}$  value of PAT against the self-aggregation of  $A\beta_{42}$  is  $12.53 \pm 1.35 \mu\text{M}$  (Fig. 2B), and the efficacy is dependent on both its concentration and reaction time (Fig. S2). This property is similar to the activity of many reported modulators such as curcumin and resveratrol that affect the fibrillogenesis of  $A\beta$  through blocking hydrophobic interactions [39]. The fluorescence intensity of ThT decreased significantly after  $A\beta_{42}$  was incubated with PAT, suggesting that the total amount of  $A\beta$  fibers was reduced.

Circular dichroism spectroscopy was used to investigate the conformational transition of  $A\beta_{42}$ , including secondary structure  $\alpha$ -helix,  $\beta$ -sheets and random coils, in the process of fibrillation [40]. As shown in Fig. 2C, a strong negative peak and a weak positive peak appeared at 217 and 203 nm after  $A\beta_{42}$  was incubated at 37 °C for 24 h, suggesting that  $\beta$ -sheets were formed in the process of self-aggregation and fibrillation. The ellipticity for the positive band increased and that for the negative band decreased after  $A\beta_{42}$  was co-incubated with  $\text{Zn}^{2+}$ , suggesting that less  $\beta$ -sheets were formed in the  $\text{Zn}^{2+}$ -induced  $A\beta$  aggregation compared to those formed in the self-aggregation, because the  $\text{Zn}^{2+}$ -induced  $A\beta$  aggregates contain both  $\beta$ -sheets and

random coils. After incubation with PAT for 24 h, the ellipticity for the negative band decreased dramatically and shifted to around 230 nm, and a broad positive band appeared, which suggest that PAT can inhibit the formation of  $\beta$ -sheets and modulate the conformation of  $A\beta_{42}$ . The morphology of  $A\beta$  aggregates were visualized by transmission electron microscope (TEM). As shown in Fig. 2D, large amounts of  $A\beta$  fibrils are formed after addition of  $Zn^{2+}$  or  $Cu^{2+}$  to  $A\beta_{40}$ , which are similar to our previous observations [41]; however, in the presence of PAT, the  $Zn^{2+}$ - or  $Cu^{2+}$ -induced  $A\beta_{40}$  aggregates or fibrils are disaggregated into granule-like species or small soluble fragments. All the results presented in Fig. 2 show that PAT can significantly inhibit the formation of aggregated  $\beta$ -sheet fibrils induced by  $A\beta$  self-aggregation and  $Zn^{2+}$  or  $Cu^{2+}$  *in vitro*.

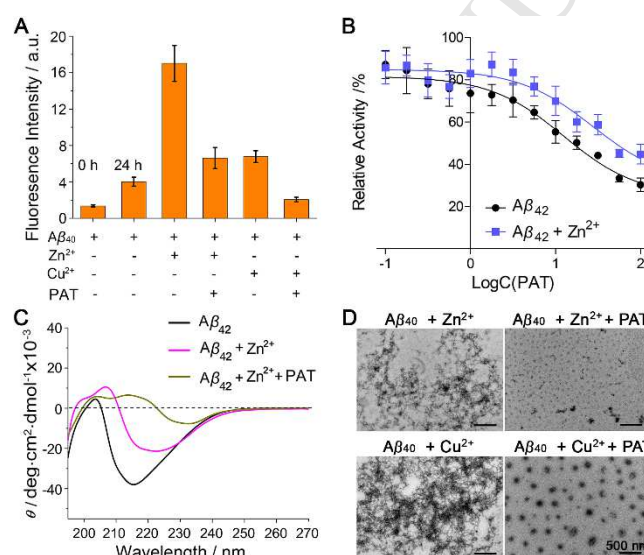


**Fig. 2.** (A) ThT fluorescence intensity ( $\lambda_{ex} = 450$  nm,  $\lambda_{em} = 485$  nm) of  $Zn^{2+}$ - or  $Cu^{2+}$  (20  $\mu$ M)-induced  $A\beta_{40}$  (20  $\mu$ M) aggregates after incubation with or without PAT (20  $\mu$ M) at 37 °C for 24 h; (B) dose-dependent inhibition of  $A\beta_{42}$  (20  $\mu$ M) aggregation by PAT in the presence or absence of  $Zn^{2+}$  (20  $\mu$ M) after incubation at 37 °C for 24 h in Tris-HCl buffer (pH 7.4); (C) conformational transition of  $A\beta_{42}$  (40  $\mu$ M) before or after treatment with PAT at 37 °C for 24 h in the presence of  $Zn^{2+}$ ,  $[A\beta_{42}]:[metal\ ion]:[chelator] = 1:1:2$ ; (D) TEM images of  $Zn^{2+}$ - or  $Cu^{2+}$ -induced  $A\beta_{40}$  aggregates incubated with or without PAT.

### 2.3. Neurotoxicity

The rat adrenal pheochromocytoma cells (PC12) can easily differentiate into neuron-like cells when treated with nerve growth factor (NGF), releasing neurotransmitter by vesicles. This makes PC12 cells useful as a model system for neuronal differentiation and neurosecretion [42]. The cell viability of PC12 cells in the presence of PAT was evaluated by the MTT assay. PAT has little toxicity to PC12 cells, in that the cell viability is  $80.50 \pm 1.86\%$  even at  $100 \mu\text{M}$  (Fig. S3).

### 2.4. Alleviation of $A\beta$ -induced paralysis in *C. elegans*

Transgenic *C. elegans* strains CL4176 and GMC101 expressing  $A\beta_{42}$  gene in the body wall muscle cells were used to determine the effects of PAT on  $A\beta$ -induced toxicity. When temperature is up-shifted from 15 to 25 °C, the deposition of  $A\beta_{42}$  aggregates would cause paralytic phenotype in CL4176 and GMC101 [23]. As shown in Fig. 3, the onset of paralysis was just started for the PAT-treated group after 33 h; meantime 80% CL4176 worms were paralyzed in the control group. The percentage of paralyzed worms were 74%, 66%, and 35% after treatment with 50, 100, and 200  $\mu\text{M}$  of PAT, respectively, for 49 h, while that of the control is 87% (Fig. 3A). The onset of paralysis in CL4176 strains was faster than in GMC101 strains, in that the percentages of the paralyzed GMC101 strains after 92 h were similar to those of CL4176 after 49 h (Fig. 3B). The results show that PAT can alleviate the  $A\beta$ -induced paralysis in both CL4176 and GMC101 strains. Under the microscope, the onset of paralysis in CL4176 strains was observed after the upshift of temperature. The worms did not move or only moved the head without PAT; after incubation with PAT, many worms still moved as a roller, which were indicated by red arrows (Fig. 3C). GMC101 strains were further tested by fluorescence imaging because  $A\beta_{42}$  and green fluorescent protein (GFP) are co-expressed in the body wall muscle (Fig. 3D). ImageJ analysis showed that the green fluorescence intensity was decreased to 43% and 20% after treatment with 50 and 100  $\mu\text{M}$  of PAT, respectively, relative to the control worms. Similarly, the fluorescence intensity was decreased in the PAT-treated CL4176 strains,

which were stained with ThT dye (Fig. S4). These results suggest that PAT could delay the onset of paralysis and reduce the  $A\beta$  deposits.

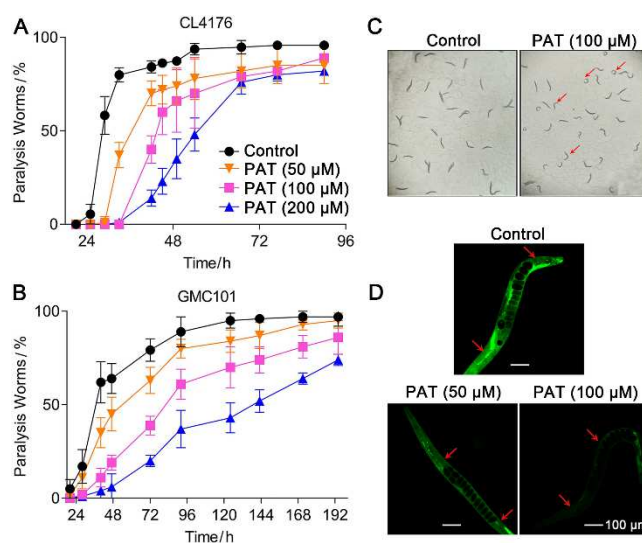


**Fig. 3.** Effect of PAT on the  $A\beta$ -induced paralysis in transgenic *C. elegans* strain CL4176 (A) and GMC101 (B), data were expressed as percentage based on three experiments ( $n = 120$ ); photos of CL4176 with or without PAT treatment at 25  $^{\circ}$ C for 48 h (C), and fluorescence confocal images of GMC101 ( $\lambda_{\text{ex}} = 488$  nm) (D), data were obtained from two experiments with 15 worms in each group.

### 2.5. Expression of $A\beta$ species in *C. elegans*

The effect of PAT on  $A\beta$  deposits in transgenic CL4176 was tested by the western blot assay. As shown in Fig. 4A, after treatment with PAT, the immunoblot showed that  $A\beta$  species (< 55 KDa), including those with low molecular weight (12, 16 KDa), were reduced significantly compared with that of the control strains. Different from the observations reported for Metformin [43] and Liuwei Dihuang [44], monomeric  $A\beta$  was not observed in the PAT-treated strains.

Although the *C. elegans* genome encodes an APP orthologue, *apl-1*, it lacks high sequence identity with  $A\beta$ , because the products of  $\beta$ -secretase activity could not be detected in *C. elegans* [19]. Thus, real-time PCR was performed to quantify the mRNA expression level of human  $A\beta$  transgene (*amy-1*). The results indicate that PAT could reduce the mRNA expression level of *amy-1* gene compared with the control

(Fig. 4B).

$A\beta$  distribution, which can be upregulated in larval animals by temperature, was further detected by fluorescence confocal imaging. Strains that stained with rhodamine-phalloidin (red) were used to visualize the actin filaments in muscle cells [45], and green fluorescence signals appeared after immunostaining with anti- $A\beta$  antibody 6E10 (Fig. 4C). As compared with the control staining, the green fluorescence intensity was decreased evidently after treatment with PAT. These results indicate that PAT could downregulate the expression of  $A\beta$  at the mRNA level and reduce the  $A\beta$  deposits in transgenic *C. elegans*.

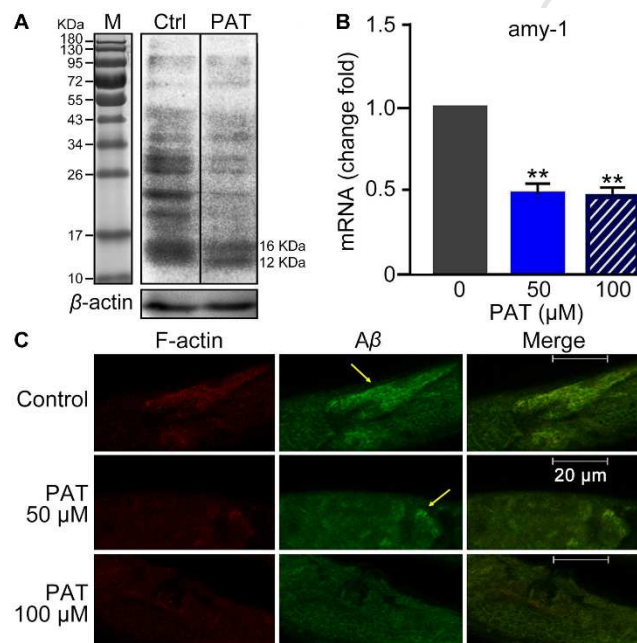


**Fig. 4.** (A) Expression of  $A\beta$  species in CL4176 worms after treatment with PAT (50  $\mu$ M) at 25 °C for 48 h, and (B) expression of gene (*amy-1*) in CL4176 worms after treatment with PAT (50, 100  $\mu$ M) at 25 °C for 48 h quantified by RT-PCR ( $2^{-\Delta\Delta Ct}$  method). The gene *ama-1* was used as the internal control; data represent an average from three independent experiments, \*\*  $p < 0.01$ . (C) Immunolocalization of anti- $A\beta$  antibody 6E10 (green) and rhodamine-phalloidin (red) in the presence or absence of PAT in CL4176 worms.

## 2.6. Antioxidant activity in *C. elegans*

$A\beta$  plaques can induce ROS accumulation and lead to oxidative stress, which can further aggravate the AD pathological progresss [46]. Therefore, the ROS level in *C. elegans* was investigated using fluorescence probe  $H_2DCF-DA$ , which reflects the ROS production by fluorescence intensity. Juglone is a superoxide-generating compound used for acute assays of oxidative stress [47]. As shown in Fig. 5, PAT (100  $\mu M$ ) suppressed the production of ROS to 21.72%, which is less than that of control (33.68%). For the juglone-stimulated group, the relative fluorescence intensity of the control group increased to 74.23%; while that of the PAT-treated (50  $\mu M$ , 100  $\mu M$ ) group decreased to 48.97% and 28.14%, respectively. These results suggest that the ROS level was significantly inhibited in the nematodes fed with PAT, and PAT can protect CL4176 against oxidative stress. The delayed onset of  $A\beta$ -related paralysis in CL4176 worms by PAT might be partly due to its antioxidant activity.

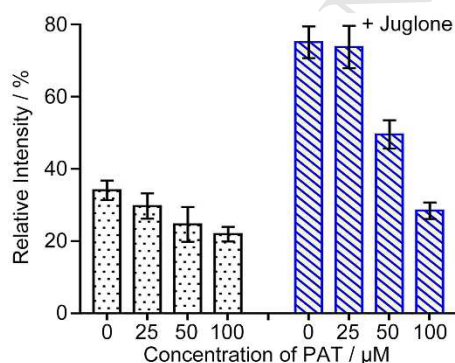


**Fig. 5.** ROS level in CL4176 worms treated with or without juglone (300  $\mu M$ ) and PAT at 48 h after upshift of temperature measured by using  $H_2DCF-DA$  fluorescence probe. Results are expressed as relative fluorescence intensity, normalized by protein concentration. Data represent mean  $\pm$  S. D., 180 worms per well, 5 wells per group.

### 2.7. Expression of stress-responsive genes in *C. elegans*

Several regulators of stress-responsive markers, including stress-induced transcription factor (*skn-1*), superoxide dismutase 3 (*sod-3*), heat shock factor (*hsf-1*), and small heat shock proteins (*hsp-16.2*, *hsp-60*), play important roles in regulating  $A\beta$  aggregation and thereby protecting *C. elegans* from  $A\beta$  toxicity [48, 49]. Thus, real time-PCR was performed using CL4176 worms to measure the gene expression

of *skn-1*, *sod-3*, *hsf-1*, *hsp-16.2* and *hsp-60*, respectively. No significant difference was observed in the expressions of *skn-1* and *sod-3*; however, the expressions of *hsf-1*, *hsp-16.2* and *hsp-60* genes were upregulated 1.55-, 2.15- and 1.59-fold, respectively, in CL4176 worms supplemented with PAT (Fig. 6). Heat shock protein (HSP) was reported to alleviate A $\beta$  toxicity by disaggregating and degrading large A $\beta$  aggregates into peptides or amino acids [50]. Surprisingly, we observed that PAT can significantly stimulate the overexpression of HSP, which may offer a protection against A $\beta$  toxicity *in vivo* by modulating oligomerization of A $\beta$  in *C. elegans*.

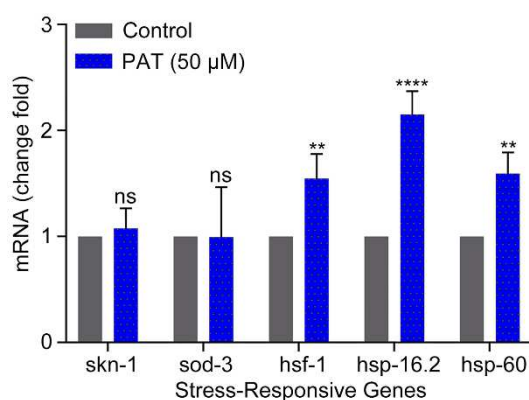


**Fig. 6.** Expression of stress-responsive genes in CL4176 worms after treatment with PAT quantified by real-time PCR ( $2^{-\Delta\Delta C_t}$  method). Gene *ama-1* was used as the internal control; data represent an average of three independent experiments, ns = not significant, \*\* $p < 0.01$ , \*\*\*\* $p < 0.0001$ .

## 2.8. Mitochondrial function

ROS accumulation could lead to oxidative damage to the mitochondria, which would reduce the viability of neuron in the AD pathological progress [51]. Thus, the effect of PAT on the oxygen consumption rate (OCR) in CL4176 worms was determined by the Seahorse XFe<sup>24</sup> Cell Bioanalyzer to evaluate the mitochondrial function. The basal respiration of the PAT-treated group is similar to that of the control group (Fig. 7). After stimulation by oligomycin (an ATP synthase inhibitor), the OCR of the control group decreased, while that of the PAT-treated group remained at the level similar to the basal respiration. The results indicate that PAT could resist

oligomycin-induced stress in the mitochondria, which ensure the level of ATP production in CL4176 strain. Therefore, PAT not only attenuates mitochondrial dysfunction, but also protects mitochondria from oxidative damage by producing less ROS in CL4176 strains.

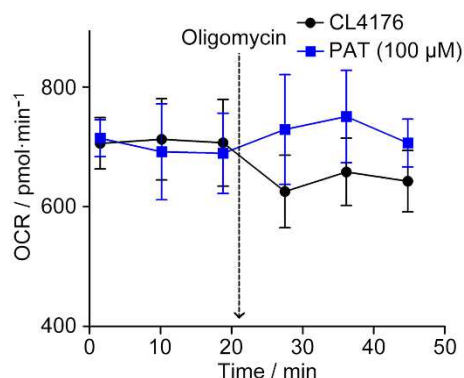


**Fig. 7.** OCR of CL4176 worms in the presence or absence of PAT before or after stimulation by oligomycin (1  $\mu\text{M}$ ) at 25  $^{\circ}\text{C}$  for 48 h (50 worms per well, 5 wells per group).

### 2.9. Acetylcholinesterase (AChE) activity in *C. elegans*

AChE is one of the most crucial enzymes for nerve response and function, which degrades the neurotransmitter acetylcholine into choline and acetic acid [52].  $A\beta$  can potently inhibit several steps of acetylcholine (ACh) synthesis and release, and decrease the availability of acetylCoA, which is also related to mitochondrial dysfunction [53]. We thus determined the activity of AChE in CL4176 strains in the presence of PAT. As shown in Table 1, the activity of AChE was reduced from 272.59 to 134.76 Units  $\text{L}^{-1}$ . However, the mRNA level of the AChE gene *ace-1* was not changed in  $A\beta$  transgenic CL4176 by PAT (Data not shown). The results suggest that PAT could inhibit the AChE activity in CL4176 strains, and thereby recovering the ACh processing, which is conducive to the alleviation of AD symptoms.

**Table 1.** The effect of PAT ( $\mu\text{M}$ ) on AChE activity (Units  $\text{L}^{-1}$ ) in CL4176 strains after treatment at 25  $^{\circ}\text{C}$  for 48 h. Data represent mean  $\pm$  S.D., normalized by protein concentration.

[PAT]	Control	25	50	100
AChE	272.59 ± 14.60	247.68 ± 11.75	166.40 ± 8.51	134.76 ± 5.95

### 2.10. Cognition and memory of APP/PS1 AD mice

AD is the most common type of neurodegenerative disease that correlates with memory deficiency and cognitive dysfunction [54]. The *in vivo* therapeutic efficacy of PAT was tested using APP/presenilin protein 1 (PS1) double-transgenic mice (9-month-old, male) as an animal model of AD. The APP/PS1 model produces elevated levels of human A $\beta$  by expressing human APP and PS1 mutant from 5 months of age [55]. The memory and cognitive abilities were assessed by Morris water maze test [56]. The learning ability of AD mice after intravenously administration of PAT or saline for 3 months were evaluated. Age-matched WT mice (9-month-old, male) were also subjected to behavioral tests as control group. The escape latency of the PAT-treated group ( $34.25 \pm 21.80$  s,  $p < 0.1$ ) is significantly shorter than that of the saline-treated group ( $50.08 \pm 17.95$  s) on day 5 (Fig. 8A). In the probe trial on day 6, the platform was removed out of the target quadrant II; the PAT-treated mice spent  $17.16 \pm 4.38$  s in the target quadrant, while the saline-treated mice almost swim around the water pool and spent  $11.77 \pm 5.28$  s in the target quadrant (Fig. 8B, Table S3). For the PAT-treated mice, the total number of crossing the hidden escape platform in the pool also increased. The results demonstrate that the cognition and memory of AD mice was effectively improved by PAT.

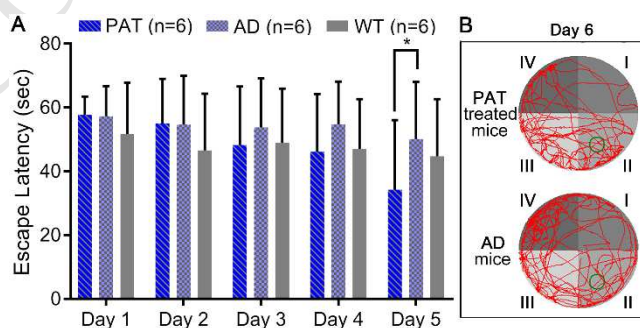


**Fig. 8.** Effects of PAT ( $1 \text{ mg kg}^{-1}$ , 15% DMSO) on double-transgenic (APP/PS1) AD mice evaluated by the Morris water maze test. (A) Escape latency time recorded daily

during training trials; data are presented as the mean  $\pm$  S. D.,  $n = 6$  each group,  $*p < 0.1$ ; (B) Swimming paths (red lines) of APP/PS1 mice ( $n = 6$  each group) with or without PAT treatment on day 6 (green circle represents the location of the platform).

### 3. Conclusions

Multifunctional small molecules could be potential drug candidates for the treatment of multifactorial diseases like AD. Based on this belief, we designed and synthesized a pyridine amine derivative (PAT) in the present study. Multifarious assays demonstrate that PAT can inhibit the self- and metal-induced  $A\beta$  aggregation, modify the conformation of  $A\beta$ , and reduce the toxicity of  $A\beta$  aggregates against neuro-like cells. *In vivo* studies on transgenic *C. elegans* carrying human  $A\beta$  gene show that PAT can down-regulate the mRNA level of human  $A\beta$  gene, reduce the expression of  $A\beta_{42}$  species, alleviate the  $A\beta$ -induced paralysis, and inhibit the AChE activity; it can also reduce the ROS level in the worms, thereby protecting them from oxidative stress and mitochondrial oxidative damage. Gene screening analyses reveal that PAT can significantly increase the mRNA level of *hsp-16.2*, *hsp-60*, and *hsf-1* genes. Particularly, induction of heat shock protein *hsp-16* expression represents a protective response to the accumulation of abnormal proteins, such as promoting  $A\beta$  sequestration, degradation, or refolding [24], which is important for mediating the tolerance to  $A\beta$  toxicity in the nematode. Last but not least, PAT can improve the cognition and memory of the APP/PS1 model mice, thus showing a promising prospect for the treatment of AD.

### 4. Experimental Section

#### 4.1. Materials and methods

Chemical reagents, including 3,5-dimethylphenol, acetic anhydride, pyridine, N-bromosuccinimide, benzoyl peroxide, triphenylphosphine, N,N-diisopropylethylamine, bis(2-pyridylmethyl)amine, thioflavin T (ThT),  $\text{CuCl}_2$ ,  $\text{ZnCl}_2$ , and 3-(4,5-dimethylthiazol-2-yl)-2,5-diphenyltetrazolium bromide (MTT)

were purchased from J&K Scientific (Beijing, China).  $A\beta_{40}$  (DAEFRHDSGYEVHHQKLVFFAEDVGSNKGAIIGLMVGGVV) and  $A\beta_{42}$  (DAEFRHDSGYEVHHQKLVFFAEDVGSNKGAIIGLMVGGVVIA) were obtained from Nanjing Taiye Company. Biological reagents, such as agar, peptone, cholesterol, yeast extract, tryptone, 5-fluoro-2'-deoxy- $\beta$ -uridine (FUdR), 2,7-dichlorofluorescein diacetate ( $H_2DCF$ -DA), 5-hydroxy-1,4-naphthalenedione (Juglone), the primary antibody of  $\beta$ -actin, oligomycin, and AChE activity kit were purchased from Sigma. The primary antibody 6E10 was purchased from Abcam (USA). HRP-conjugated goat anti-mouse antibody was purchased from Biomart (China). Alexa Fluor 488 goat anti-mouse was purchased from Molecular Probes (USA). Paraformaldehyde (4%) and triton X-100 (1%, 125 mM Tris, pH 7.4) were purchased from Byotime (China). Rhodamine-phalloidin was purchased from Cytoskeleton, Inc.. The primers used for the qRT-PCR were purchased from Genscript (China). Trizol agent was purchased from Invitrogen (USA). The iScript<sup>TM</sup> cDNA synthesis kit was purchased from Bio-Rad (USA). XFe<sup>24</sup> extracellular flux assay kit was purchased from Seahorse Bioscience (USA).

<sup>1</sup>H NMR spectra were acquired on a Bruker DRX-500 spectrometer at 298 K. Electrospray ionization mass spectra (ESI-MS) were obtained using an LCQ spectrometer (Finnigan). Fluorescence intensity was recorded using a multifunctional microplate test system (Varioskan Flash, Thermo Fisher Scientific, USA). The CD spectra were determined using a Jasco-810-150S spectropolarimeter (JASCO, Tokyo Japan). A quartz cell with a 1.0 cm optical path was used. TEM images were taken by using a JEOL JEM-2100 LaB6 (HR) transmission electron microscope (200 kV, 25000 $\times$  magnification). *C. elegans* was observed by Stereo Microscope, Motic. Fluorescence confocal imaging was carried out on a laser scanning confocal imaging system (Olympus TH4-200) consisting of ZEISS Laser Scanning Microscope (LSM 710) and a 20 mW-output 488 nm argon ion laser. Fluorescence photographs were recorded by fluorescent microscopy (Ningbo Sunny instruments Co. Ltd.). Western blotting was carried on the Bio-Rad mini-PROTEAN tetra system and Bio-Rad

Powerpack Universal. Images were captured using a Chemscope 3400 mini (Clinx science instrument co. Ltd). Quantitative real-time reverse transcription-polymerase chain reaction (qRT-PCR) was performed on the CFX96 real-time PCR detection system (Bio-Rad). Oxygen consumption rate was determined using the Seahorse XFe<sup>24</sup> instrument (Seahorse Bioscience). Morris water maze test was recorded by a video camera-based Ethovision System (Nodulus, The Netherlands).

Data were expressed as means  $\pm$  standard deviation (S. D.). Two-way Analysis of Variance (ANOVA) was used to ascertain significant differences between the controls and PAT-treated groups by the GraphPad Primer 7.00 software. Differences at the  $p \leq 0.05$  level were considered as significant.

#### 4.2. Synthesis

3,5-Bis(bromomethyl)phenyl acetate (**2**) was prepared according to the literature method with some modifications [57]. Briefly, 3,5-dimethylphenol (5.00 g, 40.93 mmol) in acetic anhydride/pyridine (1:1, 16 mL) was stirred at room temperature for 48 h, and 3,5-dimethylphenyl acetate (**1**) was obtained after removal of the solvent. Compound **1** (5.00 g, 30.45 mmol) was brominated with N-bromosuccinimide (NBS, 10.90 g, 61.24 mmol) and benzoyl peroxide (BPO, 0.28 g) in CCl<sub>4</sub> (150 mL). The exothermic reaction completed automatically after the initial heating. The mixture was filtered, and the solvent was removed to give a crude product, which was purified by SiO<sub>2</sub> column chromatography (petroleum ether/ethyl acetate, 10:1, v/v), and white solid was obtained as compound **2**. <sup>1</sup>H NMR (CDCl<sub>3</sub>, 500 MHz)  $\delta$ /ppm: 2.32 (s, 3H, -CH<sub>3</sub>), 4.45 (s, 4H, -CH<sub>2</sub>), 7.10 (d, 2H, Ph-H), 7.42–7.43 (d, 1H, Ph-H).

3-Acetoxy-5-(bromomethyl)benzyltriphenylphosphonium bromide (**3**) was prepared by dissolving **2** (1.60 g, 5.00 mmol) and triphenylphosphine (1.31 g, 5.00 mmol) in CCl<sub>4</sub> (15 mL) and stirring at room temperature overnight. The mixture was filtered and white powder product was obtained. <sup>1</sup>H NMR (CDCl<sub>3</sub>, 500 MHz)  $\delta$ /ppm: 2.20 (s, 3H, -CH<sub>3</sub>), 4.22 (s, 2H, -CH<sub>2</sub>), 5.53–5.58 (d, 2H, -CH<sub>2</sub>), 6.85–7.00 (m, 3H, Ph-H), 7.62–7.67 (m, 6H, Ph-H), 7.74–7.79 (m, 9H, Ph-H). ESI-MS (CH<sub>3</sub>CN,

positive mode,  $m/z$ ): [**3**-Br]<sup>+</sup>, found (calcd) 504.28 (504.38).

PAT was prepared as follows. *N,N*-Diisopropylethylamine (DIEA, 0.50g) and bis(2-pyridylmethyl)amine (BPA, 0.90 g, 4.50 mmol) were added into **3** (2.63 g, 4.5 mmol, 10 mL CHCl<sub>3</sub>) successively. The mixture was stirred for 2 days and the resulting DIEA salt was eliminated by filtration. The solvent in the filtrate was evaporated. The resulting oily compound **4** was stirred with methanol/water (10 mL/10 mL) and NaOH (25 mL, 40%) for 12 h. The mixture was neutralized with HCl (37%) and then extracted with CHCl<sub>3</sub>. The extraction was dried with anhydrous Na<sub>2</sub>SO<sub>4</sub>, the solvent was removed, and the crude product was purified by SiO<sub>2</sub> column chromatography (CHCl<sub>3</sub>/CH<sub>3</sub>OH, 10:1, v/v, 1% NH<sub>3</sub>·H<sub>2</sub>O). PAT was obtained as a brown powder. Yield: 60%. <sup>1</sup>H NMR (CDCl<sub>3</sub>, 500 MHz) δ/ppm: 3.23 (s, 2H, -CH<sub>2</sub>-), 3.54 (s, 4H, -CH<sub>2</sub>-), 4.64–4.69 (d, 2H, -CH<sub>2</sub>-), 6.27 (s, 1H, Ph-H), 6.88 (s, 1H, Ph-H), 7.04 (s, 1H, Ph-H), 7.10–7.14 (m, 2H, py-H), 7.46–7.71 (m, 15H, Ph-H, 4H, py-H), 8.44–8.46 (d, 2H, py-H). <sup>31</sup>P NMR (CDCl<sub>3</sub>, 202 MHz) δ/ppm: 22.51. ESI-MS (CH<sub>3</sub>OH, positive mode,  $m/z$ ): [PAT-Br]<sup>+</sup>, found (calcd) 580.58 (580.69).

#### 4.3. Inhibition of Aβ<sub>40/42</sub> aggregation

The stock solution of Aβ (200 μM) was prepared by Tris-HCl buffer (50 mM Tris, 150 mM NaCl, pH 7.4). The stock solution was dissolved with 10% NH<sub>3</sub>·H<sub>2</sub>O, diluted with ddH<sub>2</sub>O, and adjusted to pH 7.4 by HCl (1%, v/v). The concentration of Aβ was determined by Bradford assay.

Aβ<sub>40</sub> (20 μM) was incubated with CuCl<sub>2</sub> or ZnCl<sub>2</sub> (20 μM) for 5 min at room temperature; PAT (20 μM) was added and incubated at 37 °C for 24 h. Each sample was transferred to a 96-well plate, and ThT (5 μM) was added. The fluorescence intensity was recorded by a multifunctional microplate reader (λ<sub>ex</sub> = 450 nm, λ<sub>em</sub> = 485 nm). Data were expressed as mean ± standard deviations (S. D.) of at least three independent experiments.

Aβ<sub>42</sub> (20 μM) was mixed with different concentrations of PAT (0.1–100 μM) in

the presence or absence of  $\text{Zn}^{2+}$  (20  $\mu\text{M}$ ) and incubated at 37 °C for 24 h. Each sample was transferred to a 96-well plate to a final volume of 200  $\mu\text{L}$  containing ThT (5  $\mu\text{M}$ ). Samples for testing  $A\beta_{42}$  fibril formation kinetics were prepared by adding  $A\beta_{42}$  solution (200  $\mu\text{L}$ , 20  $\mu\text{M}$ ) in 96-well plates. PAT was added to the samples to obtain a final concentration of 10, 20, 40 and 60  $\mu\text{M}$ , respectively, and ThT (5  $\mu\text{M}$ ) was then added. The fluorescence intensity of these samples was monitored at 0–720 min.

$A\beta_{42}$  (40  $\mu\text{M}$ ) was incubated with  $\text{ZnCl}_2$  or  $\text{CuCl}_2$  (40  $\mu\text{M}$ ) for 5 min at room temperature; PAT (80  $\mu\text{M}$ ) was added to the solution and incubated at 37 °C for 24 h. CD spectra were determined using a Jasco-810-150S spectropolarimeter at 190–270 nm (bandwidth = 0.1 nm, response time = 10 s).

TEM samples were prepared in the same way as in the ThT assay. An aliquot of each solution (5  $\mu\text{L}$ ) was spotted on the 300-mesh carbon-coated copper grids for 2 min at room temperature and excess sample was removed. Each grid was stained with uranyl acetate (1%, w/v, 5  $\mu\text{L}$ ) for 1 min. Uranyl acetate was blotted up and the grids were dried for 20 min at room temperature. TEM images were recorded.

#### 4.4. Cytotoxicity

The rat adrenal pheochromocytoma (PC12) cells were purchased from American Type Culture Collection (ATCC). The cells were treated with nerve growth factor (NGF, Sigma) to stop dividing and promote differentiating. Highly differentiated PC12 cells were cultured over-night in RPMI-1640 medium supplement [10% heat-inactivated fetal bovine serum (v/v), 2 mM glutamine, 100 U  $\text{mL}^{-1}$  penicillin, and 100  $\mu\text{g mL}^{-1}$  streptomycin] and a highly humidified atmosphere of 95% air with 5%  $\text{CO}_2$  at 37 °C. Cell viability was measured by the MTT assay as we described previously [58]. The amount of MTT formazan was determined using a multifunctional microplate reader at 570 nm. The optical density (OD) was used to calculate the percentage of cell viability relative to the untreated control values, that is,  $(\text{OD}_{\text{test}} - \text{OD}_{\text{blank}})/(\text{OD}_{\text{control}} - \text{OD}_{\text{blank}}) \times 100\%$ , and the mean of three replicates was taken as the final result.

#### 4.5. Maintenance of *C. elegans*

Transgenic model strains CL4176 and GMC101 were obtained from the Caenorhabditis Genetics Center. The genotype of CL4176 is *smg-1(cc546) I; dvIs27 [myo-3p::A $\beta$ <sub>1-42</sub>::let-851 3'UTR + rol-6(su1006)] X*. The genotype of GMC101 is *dvIs100 [unc-54p::A $\beta$ <sub>1-42</sub>::unc-54 3'UTR + mtl-2p:GFP]*. The strains were cultured on the standard Nematode Growth Media (NGM) plates spotted with *E. coli* strain OP50 grown in Luria Broth (LB) medium. NGM (12.0 g agar, 1.5 g peptone, 1.8 g NaCl, 590 mL H<sub>2</sub>O) was autoclaved. CaCl<sub>2</sub> (0.6 mL, 1 M), cholesterol (0.6 mL, 5 mg mL<sup>-1</sup> in ethanol), MgSO<sub>4</sub> (0.6 mL, 1 M) and KPO<sub>4</sub> buffer (15.0 mL, 1 M; 17.8 g KH<sub>2</sub>PO<sub>4</sub>, 54.2 g K<sub>2</sub>HPO<sub>4</sub>, 500 mL, pH 6.0) were added to NGM. An aliquot (5.0 mL) of NGM was transferred into each petri dish ( $\phi$ 35 mm) and allowed to solidify overnight. LB medium was prepared by dissolving NaCl (10.0 g), yeast extract (5.0 g) and tryptone (10.0 g) in double distilled water (1.0 L). *E. coli* strain OP50 was grown in LB medium by shaking overnight. Each plate containing solidified NGM was spotted with 100  $\mu$ L of OP50 and allowed to dry for 4 h; it was then cultured in 37 °C overnight, cooled to room temperature and stored in 4 °C for later use.

#### 4.6. Paralysis assay

Age-synchronous worm populations of CL4176 or GMC101 were started with a synchronized parental generation, using a platinum worm picker to transfer 10 gravid adults onto several NGM plates ( $\phi$ 35 mm) spread with OP50 for laying eggs at 15 °C. The gravid adults were removed and the progenies were allowed to reach the third larval (L3); 120 worms were transferred to new plates spotted with FUdR (50  $\mu$ L, 0.5 mM). NGM plates containing PAT (50, 100 and 200  $\mu$ M) were prepared. The plates were incubated at 25 °C, a temperature at which A $\beta$ <sub>42</sub> production increases, and noted as day 0. Paralyzed worms were counted at 20 h after the initiation of temperature upshift. Nematodes that did not move or only moved the head, or failed to complete full body movement under a gentle touch with the worm picker were regarded as in paralysis. The movement of worms was observed by Stereo Microscope at the same

time. The counting continued for several hours until all worms on each plate were paralyzed. To reduce any misjudgment, the number of paralyzed worms was double-checked by two investigators independently. The results were reported as the mean value with S. D. based on the data from three independent experiments.

#### 4.7. Fluorescence imaging and ThT staining

Transgenic *C. elegans* GMC101 strains (L3) were transferred to new plates containing PAT (50, 100  $\mu$ M) and then cultured at 25 °C for 2 days; 20 of them were picked into 2% agarose pads under a glass slide. Fluorescence confocal imaging ( $\lambda_{\text{ex}} = 488$  nm,  $\lambda_{\text{em}} = 500\text{--}530$  nm) was carried out directly.

CL4176 strains (L3) were transferred to new plates containing PAT (50, 100 and 200  $\mu$ M) and then cultured at 25 °C for 2 days. Imaging was performed in triplicate with 15–20 worms per group. Worms were stained with ThT (10  $\mu$ M) for 5 min and then picked into fresh NGM plate without *E. coli* OP50. The samples of CL4176 were picked and mounted on 2% agarose pads under a glass slide after incubation for 2 h. Fluorescence photographs ( $\lambda_{\text{ex}} = 488$  nm,  $\lambda_{\text{em}} = 500\text{--}530$  nm) were taken by fluorescent microscopy (Ningbo Sunny instruments Co. Ltd.), with 1 $\times$  objective and 10 $\times$  magnification.

#### 4.8. Western blotting and immunofluorescence

CL4176 strains were synchronized and their eggs were allowed to hatch and develop to the L3 stage on NGM plates containing PAT (50  $\mu$ M) at 15 °C. The temperature was raised to 25 °C and maintained for 2 days. The worms were collected from the plates with M9 buffer and washed twice to eliminate bacteria. The final worm pellet was resuspended in phosphate buffer (200  $\mu$ L, 0.1 M), sonicated on ice for 10 s 5 times, and centrifuged at 10000 rpm for 5 min to remove insoluble debris. Total protein in the supernatant was quantified using Bradford reagent (BioRad). The protein was boiled with loading buffer at 95 °C for 5 min before being loaded into the gel. Equal amount of protein (16  $\mu$ g) was added into the lane of the 12%

Tris-Glycine-SDS-PAGE gel. Protein marker (10–180 kDa, Thermo Scientific) was used as indicator of molecular weight. Samples were run at 80 V for 30 min on stacking gel, and 120 V for 60 min on separating gel. The gel was transferred to PVDF membrane (0.22  $\mu\text{m}$ , Immobilon P, Millipore) using 20% methanol transfer buffer at 200 mA for 2 h. Blots were blocked in PBS-Tween + 5% milk for 1 h.  $A\beta$  species were detected with the primary antibody 6E10 (1:1000, Abcam), using  $\beta$ -actin (1:5000, Sigma) as a control. HRP-conjugated goat anti-mouse antibody (1:8000, Biomart) was used as the second antibody. Images were captured using a Chemscope 3400 mini.

CL4176 strains (L3) were cultured on NGM plates containing PAT (50,100  $\mu\text{M}$ ) at 25 °C for 2 days, collected, rinsed and fixed in 4% paraformaldehyde overnight. After fixation, worms were rinsed twice with PBS and permeabilized by 1% Triton X-100 (125 mM Tris, pH 7.4).  $A\beta$  species was detected with the primary monoclonal antibody 6E10, and maintained by the Alexa Fluor 488 goat anti-mouse (Molecular Probes) secondary antibody. Samples were also stained with rhodamine-phalloidin (1:4000) for the visualization of actin filaments in muscle cells. The animals were mounted on 2% agarose pads, covered with a cover slip and sealed. The samples were photographed by a ZEISS Laser Scanning Microscope (LSM 710) at  $\lambda_{\text{ex}} = 488 \text{ nm}$ ,  $\lambda_{\text{em}} = 500\text{--}530 \text{ nm}$  (Alexa Fluor 488); or at  $\lambda_{\text{ex}} = 543 \text{ nm}$ ,  $\lambda_{\text{em}} = 565\text{--}605 \text{ nm}$  (rhodamine).

#### 4.9. RNA Extraction and qRT-PCR

RNA was prepared using Trizol reagent (Invitrogen) and stored at  $-80 \text{ }^{\circ}\text{C}$ . Complementary DNA was prepared by using iScript<sup>TM</sup> cDNA synthesis kit (Bio-Rad). The qRT-PCR was performed using SsoFast EvaGreen Supermix (Bio-Rad) and according to the protocol suggested by the manufacturer: 30 s at 95 °C, followed by 40 cycles of 5 s at 95 °C, and 5 s at 60 °C. *Ama-1* was used as an internal control to normalize the expression level of target transcripts. Relative fold changes for transcripts were calculated using the comparative CT ( $2^{-\Delta\Delta\text{CT}}$ ) method. Each qRT-PCR

experiment was repeated three times by independent RNA/cDNA preparations. *A $\beta$*  transgene (*amy-1*), stress induced transcription factor (*skn-1*), superoxide dismutase 3 (*sod-3*), small heat shock protein (*hsp-16.2* and *hsp-60*), and heat shock factor (*hsf-1*) were subjected to qRT-PCR, and the transcript quantity was normalized using the actin genes (*ama-1*) [59]. Samples were run in triplicate (n = 3), and the primers used for the qRT-PCR were shown in Table S2.

#### 4.10. Measurement of ROS in *C. elegans*

Intracellular ROS in CL4176 strains was measured using H<sub>2</sub>DCF-DA. Freshly laid CL4176 eggs (100 eggs per plate) were transferred to NGM plates containing PAT (0, 25, 50, 100  $\mu$ M) and incubated at 15 °C. The temperature was raised to 25 °C for 48 h. The worms were collected by M9 buffer, washed twice with PBS to remove *E. coli* OP50, transferred to a 96-well plate (Costar) with 200  $\mu$ L of PBS containing Tween 20 (0.01%), and H<sub>2</sub>DCF-DA (100  $\mu$ M) was added. In the parallel experiment for determining the oxidative stress tolerance, juglone (300  $\mu$ M) was added, and the fluorescence intensity ( $\lambda_{\text{ex}} = 485$  nm,  $\lambda_{\text{em}} = 530$  nm) was quantified by a microplate reader after 6 h. Data were represented as mean  $\pm$  S.D., n = 3.

#### 4.11. Oxygen consumption rate (OCR)

CL4176 strains were synchronized, treated with or without PAT (100  $\mu$ M) at 25 °C for 48 h. The worms were picked to new NGM plates with no bacteria, washed with M9 and put into the XF 24-well plates 50 worms per well. Experiments were repeated three times with 5 wells under each condition. Before measurement on the Seahorse XFe<sup>24</sup> instrument, the culture medium was changed with XFe<sup>24</sup> extracellular flux assay medium. OCR was read using the following settings: 5 cycles of mixing (30 s), waiting (30 s) and measuring (3 min). Oligomycin (1  $\mu$ M) was added after the detection of basal respiration. Each experiment was repeated three times.

#### 4.12. Activity of acetylcholinesterase

Fresh lysates from the CL4176 worms after treatment with PAT (0, 25, 50, 100

$\mu\text{M}$ ) at 25 °C for 48 h were prepared by sonication in phosphate buffer (0.1 M, pH 7.4), followed by centrifugation at 13000 rpm for 5 min, and collection of the supernatants. AChE activity kit (Sigma) was used to quantify the thiocholine produced in the hydrolysis of acetylthiocholine by AChE in worm extracts. The absorption of DTNB adduct was used to measure the amount of thiocholine, which is proportional to the AChE activity. The kit provides a colorimetric one-step assay to detect 10–600 units/L AChE. The signal was read by an absorbance microplate reader at 412 nm.

#### 4.13. Animal studies

Double transgenic AD mice, B6C3-Tg (APP<sup>swe</sup>, PSEN1<sup>dE9</sup>)85Dbo/J (male, 3 months old, 30–45 g, n = 12), were purchased from the Guangdong Medical Laboratory Animal Center. The APP/PS1 mice were randomly allocated into two groups (n = 6 for each group) when they were 6-month old, and intravenously administered with PAT (1 mg kg<sup>-1</sup>, 15% DMSO) or saline containing 15% DMSO every three days, lasted for 3 months. Wildtype C57BL/6 mice (male, 8 months old, 20–25 g, n = 6) were purchased from the Model Animal Research Center of Nanjing University. The mice were fed in individual cages at 23 °C, with ad libitum access to sterile food and water. All experimental procedures on animals were approved by the Model Animal Research Center of Nanjing University.

#### 4.14. Morris water maze test

The learning and cognitive abilities of AD mice (9-month old) were assessed by the Morris water maze test following the procedures reported in the literature [56]. The test consisted of 4 platform trials per day for consecutive 5 days, and followed by a probe trial on the 6th day. In platform trials, the distance of path and escape latency were measured. After training, the mice were tested to search for the platform in the Morris water maze apparatus, in which they were permitted to swim freely for 60 s. In probe trials, the swimming path were recorded by a video camera-based Ethovision System (Nodulus, the Netherlands). The daily test data were analyzed statistically.

The data for escape latency, the traveled distances, and the number of times for crossing platform region were recorded in Table S3.

### **Acknowledgements**

This work was supported by the National Natural Science Foundation of China (Grants 31700714, 21877059, 81671390), the National Postdoctoral Program for Innovative Talents (BX201600069), the China Postdoctoral Science Foundation (2017M611777), and the State Key Laboratory of Pharmaceutical Biotechnology of Nanjing University (grant number: 02ZZYJ-201302).

### **Appendix A. Supplementary data**

Supplementary data to this article can be found XXX

### **References**

- [1] C. Patterson, World Alzheimer Report 2018-The state of the art of dementia research: New frontiers, *Alzheimer's Disease International* 2018.
- [2] Alzheimer's Association, 2018 Alzheimer's disease facts and figures, *Alzheimers. Dement.* 14 (2018) 367-429.
- [3] W. V. Graham, A. Bonito-Oliva, T. P. Sakmar, Update on Alzheimer's disease therapy and prevention strategies, *Annu. Rev. Med.* 68 (2017) 413-430.
- [4] S. O. Bachurin, E. V. Bovina, A. A. Ustyugov, Drugs in clinical trials for Alzheimer's disease: the major trends, *Med. Res. Rev.* 37 (2017) 1186-1225.
- [5] J. L. Cummings, T. Morstorf, K. Zhong, Alzheimer's disease drug-development pipeline: few candidates, frequent failures, *Alzheimers Res. Ther.* 6 (2014) 1-7.
- [6] L. Ghezzi, E. Scarpini, D. Galimberti, Disease-modifying drugs in Alzheimer's disease, *Drug Des. Dev. Ther.* 7 (2013) 1471-1479.
- [7] Y. Huang, L. Mucke, Alzheimer mechanisms and therapeutic strategies, *Cell* 148 (2012) 1204-1222.
- [8] A. H. Bhat, K. B. Dar, S. Anees, M. A. Zargar, A. Masood, M. A. Sofi, S. A. Ganie. Oxidative stress, mitochondrial dysfunction and neurodegenerative diseases; a mechanistic insight. *Biomed. Pharmacother.* 74 (2015) 101-110.
- [9] M. P. Murphy, H. LeVine, III, Alzheimer's disease and the amyloid-beta peptide, *J. Alzheimers Dis.* 19 (2010) 311-323.

- [10] S. A. Kotler, P. Walsh, J. R. Brender, A. Ramamoorthy, Differences between amyloid-[small beta] aggregation in solution and on the membrane: insights into elucidation of the mechanistic details of Alzheimer's disease, *Chem. Soc. Rev.* 43 (2014) 6692-6700.
- [11] F. M. LaFerla, K. N. Green, S. Oddo, Intracellular amyloid-beta in Alzheimer's disease, *Nat. Rev. Neurosci.* 8 (2007) 499-509.
- [12] K. L. Viola, W. L. Klein, Amyloid beta oligomers in Alzheimer's disease pathogenesis, treatment, and diagnosis, *Acta Neuropathol.* 129 (2015) 183-206.
- [13] E. S. Musiek, D. M. Holtzman. Three dimensions of the amyloid hypothesis: time, space and 'wingmen', *Nat. Neurosci.* 18 (2015) 800-806.
- [14] K. P. Kepp, Alzheimer's disease: how metal ions define beta-amyloid function, *Coord. Chem. Rev.* 351 (2017) 127-159.
- [15] F. Hane, Z. Leonenko, Effect of metals on kinetic pathways of amyloid-beta aggregation, *Biomolecules* 4 (2014) 101-116.
- [16] A. S. Pithadia, M. H. Lim, Metal-associated amyloid-beta species in Alzheimer's disease, *Curr. Opin. Chem. Biol.* 16 (2012) 67-73.
- [17] M. P. Murphy, Amyloid-beta solubility in the treatment of Alzheimer's disease, *N. Engl. J. Med.* 378 (2018) 391-392.
- [18] Q. Wang, X. Yu, L. Li, J. Zheng, Inhibition of amyloid-beta aggregation in Alzheimer's disease, *Curr. Pharm. Design* 20 (2014) 1223-1243.
- [19] A. G. Alexander, V. Marfil, C. Li, Use of *Caenorhabditis elegans* as a model to study Alzheimer's disease and other neurodegenerative diseases, *Front. Genet.* 5 (2014) [Article 279].
- [20] L. Ma, Y. D. Zhao, Y. C. Chen, B. Cheng, A. D. Peng, K. Huang, *Caenorhabditis elegans* as a model system for target identification and drug screening against neurodegenerative diseases, *Eur. J. Pharmacol.* 819 (2018) 169-180.
- [21] B. V. Nia, C. Kang, M. G. Tran, D. Lee, S. Murakami, Meta analysis of human AlzGene database: benefits and limitations of using *C. elegans* for the study of Alzheimer's disease and co-morbid conditions, *Front. Genet.* 8 (2017) [Article 55].
- [22] G. McColl, B. R. Roberts, T. L. Pukala, V. B. Kenche, C. M. Roberts, C. D. Link, T. M. Ryan, C. L. Masters, K. J. Barnham, A. I. Bush, R. A. Cherny, Utility of an improved model of amyloid-beta ( $A\beta_{1-42}$ ) toxicity in *Caenorhabditis elegans* for drug screening for Alzheimer's disease, *Mol. Neurodegener.* 7 (2012) 57.
- [23] A. L. Lublin, C. D. Link, Alzheimer's disease drug discovery: in vivo screening using *Caenorhabditis elegans* as a model for  $\beta$ -amyloid peptide-induced toxicity, *Drug Discov Today Technol.* 10 (2013) e115-e119.
- [24] V. Fonte, D. R. Kipp, J. Yerg, III, D. Merin, M. Forrestal, E. Wagner, C. M. Roberts, C. D. Link, Suppression of in vivo beta-amyloid peptide toxicity by overexpression of the HSP-16.2 small chaperone protein, *J. Biol. Chem.* 283 (2008) 784-791.

- [25] Y. J. Wu, Z. M. Cao, W. L. Klein, Y. Luo, Heat shock treatment reduces beta amyloid toxicity in vivo by diminishing oligomers, *Neurobiol. Aging* 31 (2010) 1055-1058.
- [26] M. A. Santos, K. Chand, S. Chaves, Recent progress in multifunctional metal chelators as potential drugs for Alzheimer's disease, *Coord. Chem. Rev.* 327 (2016) 287-303.
- [27] A. K. Sharma, S. T. Pavlova, J. Kim, D. Finkelstein, N. J. Hawco, N. P. Rath, J. Kim, L. M. Mirica, Bifunctional compounds for controlling metal-mediated aggregation of the  $A\beta_{42}$  peptide, *J. Am. Chem. Soc.* 134 (2012) 6625-6636.
- [28] M. P. Murphy, Targeting lipophilic cations to mitochondria, *Biochim. Biophys. Acta -Bioenerg.* 1777 (2008) 1028-1031.
- [29] J. Zielonka, J. Joseph, A. Sikora, M. Hardy, O. Ouari, J. Vasquez-Vivar, G. Cheng, M. Lopez, B. Kalyanaraman, Mitochondria-targeted triphenylphosphonium-based compounds: syntheses, mechanisms of action, and therapeutic and diagnostic applications, *Chem. Rev.* 117 (2017) 10043-10120.
- [30] R. A. J. Smith, M. P. Murphy, Animal and human studies with the mitochondria-targeted antioxidant MitoQ, *Ann. N.Y. Acad. Sci.* 1201 (2010) 96-103.
- [31] J. K. Romary, J. D. Barger, J. E. Bunds, New multidentate  $\alpha$ -pyridyl ligand. Coordination of bis(2-pyridylmethyl)amine with transition metal ions, *Inorg. Chem.*, 7 (1968) 1142-1145.
- [32] L. Q. Hatcher, L. Hong, W. D. Bush, T. Carducci, J. D. Simon, Quantification of the binding constant of copper(II) to the amyloid-beta peptide, *J. Phys. Chem. B*, 112 (2008) 8160-8164.
- [33] V. Tōugu, A. Karafin, P. Palumaa, Binding of zinc(II) and copper(II) to the full-length Alzheimer's amyloid-b peptide, *J. Neurochem.*, 104 (2008) 1249-1259.
- [34] M. F. Ross, G. F. Kelso, F. H. Blaikie, A. M. James, H. M. Cocheme, A. Filipovska, T. Da Ros, T. R. Hurd, R. A. Smith, M. P. Murphy, Lipophilic triphenylphosphonium cations as tools in mitochondrial bioenergetics and free radical biology, *Biochemistry (Mosc.)* 70 (2005) 222-230.
- [35] C. A. Lipinski, F. Lombardo, B. W. Dominy, P. J. Feeney, Experimental and computational approaches to estimate solubility and permeability in drug discovery and development, *Adv. Drug Deliv. Rev.* 46 (2001) 3-26.
- [36] R. D. Broadwell, M. Salzman, R. S. Kaplan, Morphologic effect of dimethyl sulfoxide on the blood-brain barrier. *Science* 217 (1982) 164-166.
- [37] S. Noel, S. Cadet, E. Gras, C. Hureau, The benzazole scaffold: a SWAT to combat Alzheimer's disease, *Chem. Soc. Rev.* 42 (2013) 7747-7762.
- [38] E. Karran, M. Mercken, B. D. Strooper, The amyloid cascade hypothesis for Alzheimer's disease: an appraisal for the development of therapeutics, *Nat. Rev. Drug Discov.* 10 (2011) 698-712.
- [39] C. J. Lu, Y. Y. Guo, J. Yan, Z. H. Luo, H.-B. Luo, M. Yan, L. Huang, X. S. Li, Design, Synthesis, and evaluation of multitarget-directed resveratrol derivatives for the treatment of Alzheimer's disease, *J. Med. Chem.* 56 (2013) 5843-5859.

- [40] Y. Y. Cao, L. Wang, Z. X. Lin, F. Y. Liang, Z. Pei, J. Xu, Q. Gu, Dehydroabietylamine derivatives as multifunctional agents for the treatment of Alzheimer's disease, *Med. Chem. Commun.* 5 (2014) 1736-1743.
- [41] X. Ma, J. A. Hua, K. Wang, H. M. Zhang, C. L. Zhang, Y. F. He, Z. J. Guo, X. Y. Wang, Modulating conformation of A $\beta$ -peptide: an effective way to prevent protein-misfolding disease, *Inorg. Chem.* 57 (2018) 13533-13543.
- [42] R. H. S. Westerink, A. G. Ewing, The PC12 cell as model for neurosecretion, *Acta Physiol.* 192 (2008) 273-285.
- [43] W. Ahmad, P. R. Ebert, Metformin attenuates a beta pathology mediated through levamisole sensitive nicotinic acetylcholine receptors in a C-elegans model of Alzheimer's disease, *Mol. Neurobiol.* 54 (2017) 5427-5439.
- [44] J. S. Sangha, X. L. Sun, O. S. D. Wally, K. B. Zhang, X. H. Ji, Z. M. Wang, Y. W. Wang, J. Zidichouski, B. Prithiviraj, J. Z. Zhang, Liuwei Dihuang (LWDH), a traditional Chinese medicinal formula, protects against beta-amyloid toxicity in transgenic *Caenorhabditis elegans*, *Plos One* 7 (2012) e43990.
- [45] A. N. Minniti, D. L. Rebolledo, P. M. Grez, R. Fadic, R. Aldunate, I. Volitakis, R. A. Cherny, C. Opazo, C. Masters, A. I. Bush, N. C. Inestrosa, Intracellular amyloid formation in muscle cells of A beta-transgenic *Caenorhabditis elegans*: determinants and physiological role in copper detoxification, *Mol. Neurodegener.* 4 (2009) 2.
- [46] S. Gandhi, A. Y. Abramov, Mechanism of oxidative stress in neurodegeneration, *Oxidative Med. Cell. Longev.* 2012 (2012) 1-11.
- [47] T. A. Crombie, L. Tang, K. P. Choe, D. Julian, Inhibition of the oxidative stress response by heat stress in *Caenorhabditis elegans*, *J. Exp. Biol.* 219 (2016) 2201-2211.
- [48] D. J. Dues, E. K. Andrews, C. E. Schaar, A. L. Bergsma, M. M. Senchuk, J. M. Van Raamsdonk, Aging causes decreased resistance to multiple stresses and a failure to activate specific stress response pathways, *Aging* 8 (2016) 777-795.
- [49] V. Dostal, C. M. Roberts, C. D. Link, Genetic mechanisms of coffee extract protection in a *Caenorhabditis elegans* model of beta-amyloid peptide toxicity, *Genetics* 186 (2010) 857-866.
- [50] E. Cohen, J. Bieschke, R. M. Perciavalle, J. W. Kelly, A. Dillin, Opposing activities protect against age-onset proteotoxicity, *Science* 313 (2006) 1604-1610.
- [51] I. Piaceri, V. Rinnoci, S. Bagnoli, Y. Failli, S. Sorbi, Mitochondria and Alzheimer's disease, *J. Neurol. Sci.* 322 (2012) 31-34.
- [52] V. N. Talesa, Acetylcholinesterase in Alzheimer's disease, *Mech. Ageing Dev.* 122 (2001) 1961-1969.
- [53] D. S. Auld, S. Kar, R. Quirion,  $\beta$ -Amyloid peptides as direct cholinergic neuromodulators: a missing link, *Trends Neurosci.* 21 (1998) 43-49.

- [54] M. Ishii, C. Iadecola, Metabolic and non-cognitive manifestations of Alzheimer's disease: the hypothalamus as both culprit and target of pathology, *Cell Metab.* 22 (2015) 761-776.
- [55] H. Y. Kim, H. V. Kim, S. Jo, C. J. Lee, S. Y. Choi, D. J. Kim, Y. S. Kim, EPPS rescues hippocampus-dependent cognitive deficits in APP/PS1 mice by disaggregation of amyloid-beta oligomers and plaques, *Nat. Commun.* 6 (2015) 8997.
- [56] X. M. Zha, D. Lamba, L. L. Zhang, Y. H. Lou, C. X. Xu, D. Kang, L. Chen, Y. G. Xu, L. Y. Zhang, A. De Simone, S. Samez, A. Pesaresi, J. Stojan, M. G. Lopez, J. Egea, V. Andrisano, M. Bartolini, Novel Tacrine-benzofuran hybrids as potent multitarget-directed ligands for the treatment of Alzheimer's disease: design, synthesis, biological evaluation, and X-ray crystallography, *J. Med. Chem.* 59 (2016) 114-131.
- [57] X. D. Dong, X. Y. Wang, M. X. Lin, H. Sun, X. L. Yang, Z. J. Guo, Promotive effect of the platinum moiety on the DNA cleavage activity of copper-based artificial nucleases, *Inorg. Chem.* 49 (2010) 2541-2549.
- [58] Z. Z. Zhu, Z. H. Wang, Y. G. Hao, C. C. Zhu, Y. Jiao, H. C. Chen, Y.-M. Wang, J. Yan, Z. J. Guo, X. Y. Wang, Glutathione boosting the cytotoxicity of a magnetic platinum(IV) nano-prodrug in tumor cells, *Chem. Sci.* 7 (2016) 2864-2869.
- [59] J. S. Sangha, O. Wally, A. H. Banskota, R. Stefanova, J. T. Hafting, A. T. Critchley, B. Prithiviraj, A cultivated form of a red seaweed (*Chondrus crispus*), suppresses  $\beta$ -amyloid-induced paralysis in *Caenorhabditis elegans*, *Mar. Drugs* 13 (2015) 6407-6424.

# Inhibiting $A\beta$ toxicity in Alzheimer's disease by a pyridine amine derivative

Zhenzhu Zhu<sup>a,#</sup>, Tao Yang<sup>a,#</sup>, Lei Zhang<sup>a</sup>, Lulu Liu<sup>a</sup>, Enmao Yin<sup>a</sup>, Changli Zhang<sup>b</sup>, Zijian Guo<sup>c</sup>, Chen Xu<sup>a,\*</sup>, and Xiaoyong Wang<sup>a,\*</sup>

<sup>a</sup> State Key Laboratory of Pharmaceutical Biotechnology, School of Life Sciences, Nanjing University, Nanjing 210023, P. R. China

<sup>b</sup> Department of Chemistry, Nanjing Xiaozhuang College, Nanjing 210017, P. R. China

<sup>c</sup> State Key Laboratory of Coordination Chemistry, School of Chemistry and Chemical Engineering, Nanjing University, Nanjing 210023, P. R. China

\* Corresponding author. E-mail addresses: boxwxy@nju.edu.cn (X. Y. Wang); xuchn@nju.edu.cn (C. Xu)

# These authors contributed equally to this work.

## HIGHLIGHTS

- Multifunctional pyridine amine derivative (PAT) inhibits  $A\beta$  aggregation in vitro.
- PAT alleviates the  $A\beta$ -induced paralysis and production of ROS in *C. elegans*.
- PAT up-regulates the expression of heat shock proteins in *C. elegans*.
- PAT reduces the activity of acetylcholinesterase in *C. elegans*.
- PAT improves the cognition and memory of Alzheimer's disease model mice.